Expanding MISR LAI Products to High Temporal Resolution With MODIS Observations

Yang Liu, *Member, IEEE*, Ronggao Liu, *Member, IEEE*, Jing M. Chen, and Weimin Ju

***Abstract*—The Multi-Angle Imaging Spectroradiometer (MISR) is a powerful sensor for leaf area index (LAI) mapping with its simultaneous multi-angle observations. However, the LAI product derived from MISR observations has low temporal resolution, which is unsatisfactory for many applications. This paper presents an algorithm that expands the MISR LAI product to high temporal resolution with the aid of Moderate Resolution Imaging Spectroradiometer (MODIS) data. The algorithm establishes relationships between the MISR LAI and the MODIS red/near-infrared band ratio (simple ratio (SR)) pixel by pixel using coincident data of these two sensors for the past nine years. Using these pixel-based SR-LAI relationships, a new LAI product with the merits of the original MISR product and high temporal resolution is obtained from MODIS surface reflectance. The expanded LAI series was compared with the original MISR and MODIS LAI products, as well as field LAI measurements made at the Baohe and Maoershan forest sites and the Hulunbeier grassland site, to assess the algorithm's performance. The results show that the temporal coverage of the MISR LAI improved from 15.5% to 65.2% in an 8-day composite, and the mean root-mean-square error is 0.74 for the vegetated pixels. This LAI product has similar temporal consistency and seasonal dynamics to the existing MODIS LAI product generated from the main algorithm, but is more robust against the low quality of reflectance inputs. The expanded LAI product differs with field measurements by about 11.5%, with agreement to field observations at all three sites within an accuracy of 0.8 LAI.**

***Index Terms*—Interpolation, inversion problems, leaf area index (LAI), remote sensing.**

I. Introduction

THE LEAF area index (LAI), which is commonly defined as half the total developed area of green leaves per unit ground surface area [1] is an indispensable input that characterizes the vegetation structure in most climate, hydrology, biogeochemistry, and ecosystem models [2]. Large-area LAI mapping is essential in research on the global carbon cycle and climate change [3].

Remote sensing is a powerful tool for estimating the LAI over large region [4]. Several standard products of the global LAI have been routinely provided, such as Moderate Resolution Imaging Spectroradiometer (MODIS) [3], VEGETATION [5], [6] and MERIS LAI products [7]. These products provide global time series of LAI data sets for characterizing vegetation dynamics. However, they are produced from observations with a single view, which means more assumptions are needed to constrain the inversion models. Although multi-angle measurements can also be acquired through the accumulation of observations over a period of several days, cloud is likely to affect the acquisition of multi-angle imagery, the surface may change during the accumulation period, and the footprint size is different for each view [8].

Multi-angle remote sensing provides abundant information for LAI mapping [9]–[11]. The Multi-Angle Imaging Spectroradiometer (MISR), which is a major multi-angle instrument onboard the Terra satellite and measures the earth's spectral radiance in four spectral bands at nine viewing angles in the forward and backward directions along the flight path, is an excellent candidate for LAI retrieval [12]. An LAI product is routinely produced from MISR data through the inversion of a 3-D radiative transfer model, which constrains the retrieval behaviors using multi-angular reflectance without a prescribed biome map [13]. In addition, the anisotropy measurements of MISR could be applied to discriminate canopy structures and separate the contribution of overstory canopy and background reflectance, which would further improve LAI retrieval [8], [14], [15]. However, it takes 9 days for the MISR to acquire global coverage. This temporal resolution is insufficient for many applications. To broaden the applications of the MISR LAI product, it is essential to improve its temporal resolution.

Quantitative fusion of MISR data with those remote sensing observations with high temporal resolution may be a feasible method to expand the MISR LAI product to high temporal resolution. The MODIS, which is onboard the same satellite as the MISR, provides global observations every 1 to 2 days. The swath of the MISR (360 km) is covered entirely by that of MODIS (2330 km), making it possible to improve the temporal resolution of MISR LAI data with the aid of MODIS data. If the relationship between MODIS observations and MISR LAI can be established, it is expected that the LAI estimated from MODIS observations using this relationship would keep the merits of MISR LAI and the high temporal resolution of MODIS. It is well known that the LAI is highly correlated with vegetation indices (VIs). Among various VIs, simple ratio

Manuscript received December 19, 2010; revised June 20, 2011, October 27, 2011, and December 31, 2011; accepted January 15, 2012. Date of publication March 9, 2012; date of current version September 21, 2012. This work was supported by the China 973 program (2010CB950701), the R&D Special Fund for Public Welfare Industry (meteorology) (GYHY201106014), and the National Natural Science Foundation from China (41171285).

Y. Liu is with the Institute of Geographic Sciences and Natural Resources Research, Chinese Academy of Sciences, Beijing 100101, China, and also with the Graduate University of Chinese Academy of Sciences, Beijing 100049, China (e-mail: liuyang@lreis.ac.cn).

R. Liu is with the Institute of Geographic Sciences and Natural Resources Research, Chinese Academy of Sciences, Beijing 100101, China (email: liurg@igsnrr.ac.cn).

J. M. Chen and W. Ju are with the International Institute for Earth System Science, Nanjing University, Nanjing 210093, China (e-mail: jing.chen@utoronto.ca; juweimin@nju.edu.cn).

Color versions of one or more of the figures in this paper are available online at http://ieeexplore.ieee.org.

Digital Object Identifier 10.1109/TGRS.2012.2185828

(SR), the ratio of the near-infrared to red band land surface reflectance, has been extensively applied to LAI retrieval owing to its simplicity and approximate linearity with the LAI [2], [16]. However, the SR-LAI relationship is site dependent. If the site-dependent relationships were established, they would be a feasible means for expanding the MISR LAI to high temporal resolution.

In this paper, an algorithm for expanding the MISR LAI product (hereinafter the MISR LAI expanding algorithm) using MODIS measurements and pixel-level SR-LAI relationships is proposed. The relationships are developed by combining the MISR LAI with calculated MODIS SR. The LAI with high temporal resolution (hereinafter the expanded LAI) is then retrieved from MODIS surface reflectance using these pixel-level relationships. To account for the effect of angular variations on MODIS observations, pixel-by-pixel SR-bidirectional reflectance factor (BRF) model parameters relationships are also calculated on the basis of the MISR BRF model parameter products and the coincident MODIS land surface reflectance [13]. The algorithm was applied to the entire mainland of China. The results were compared with the original MISR and MODIS LAI products to evaluate the retrieval capability, temporal consistency, and possible biases of the proposed algorithm. Furthermore, the expanded LAI was evaluated against field LAI measurements made over Baohe, Maoershan, and Hulunbeier sites.

This paper is organized as follows. Section II describes the MISR and MODIS data used in this study. Section III presents the algorithm in detail. Section IV presents the results of the algorithm applied to China, and evaluates the retrieval capability, temporal consistency, and biases of the proposed algorithm results by comparing with the existing MISR and MODIS LAI products. The validation of the expanded LAI product against LAI measurements in several areas in China and analysis of BRDF effects are also presented in Section IV. The limitation and potential improvements of the algorithm are discussed in Section V. Finally, concluding remarks are given in Section VI.

II. Data

Several MODIS and MISR data sets covering a 9-year period from 2000 to 2008 were used. The daily SR maps were calculated from MODIS daily land surface reflectance products (MOD09GA). The pixel-level SR-LAI relationship was established from the daily MISR LAI products and the coincident MODIS SR. A pixel-level SR-BRF model parameters relationship (hereinafter referred to as the SR-BRDF relationship) database was established from the MISR BRF model parameters and MODIS SR. The expanded LAI was retrieved from the 8-day composite MODIS land surface reflectance MOD09A1 products for 2000–2008 according to pixel-level SR-LAI relationships. The performance of the algorithm was evaluated with the MODIS LAI product MOD15A2, the MISR LAI, and local fine-resolution LAI maps.

MISR LAI and BRF model parameters products are included in the Level 2 Land Surface product (MIL2ASLS) with a resolution of 1.1 km. The three BRF model parameters for the four MISR wavelengths are determined by inverting the modified Rahman model [17]. The MISR LAI product was shown to have structural and phenological variability similar to MODIS LAI data with biases within 0.66 for herbaceous vegetation and savannas and to be overestimated by about 1.0 for broadleaf forests [18]. The global MISR LAI and BRF model parameters data sets are provided in the HDF-EOS "stacked-block" grid format in 233 paths. All MISR data were downloaded from http://l0dup05.larc.nasa.gov/.

The MODIS Surface Reflectance Product (MOD09) contains seven surface reflectance bands. MOD09GA and MOD09A1 provide global daily and the 8-day composite land surface reflectance at 500 m resolution, respectively. The MODIS global LAI Collection 5 product (MOD15) contains the global 8-day composite LAI of the land surface in 1 km $\times$ 1 km grid generated from the inversion of a 3-D radiative transfer model [3]. If the main algorithm fails, a backup algorithm based on the relationship between the LAI and Normalized Difference Vegetation Index (NDVI) is used. All MODIS data were downloaded from https://wist.echo.nasa.gov/api/.

III. Method

A. SR-LAI Relationship Analysis

The reflectance in a few bands, such as the red and near-infrared bands, are generally combined as VIs to minimize the influence of soil reflectance and atmospheric effects on spectral data and to derive LAI and other canopy characteristics [19]. SR, one of the most popular VIs, is closely correlated with ground measurements of the LAI and suitable for LAI retrieval for various biomes, including grassland, cropland, and coniferous and deciduous forests (e.g., [20]–[24]). It has been applied in regional and global LAI retrieval owing to its high sensitivity and approximate linearity with the LAI [2], [5], [25]. To demonstrate the relationship between the LAI and SR, the time series of daily SR from MODIS MOD09GA and MISR LAI data from 2000 to 2008 for several typical sites in China that cover the main biome types were shown as examples (Fig. 1). The regression relations between the LAI and SR show good linearity, but the coefficients vary for different sites. This indicates the necessity of establishing a pixel-based SR-LAI relationship for LAI retrieval. The LAI of grassland, cereal crop, shrubland, and broadleaf crop are more significantly related to SR with the R^2 of 0.90, 0.91, 0.91, and 0.87, respectively. While the LAI of forest, particularly needleleaf forest do not show significant linear relationships to SR, which may due to the provisional quality level of MISR LAI data set for needleleaf forest [13]. The statistics of global regression residuals over the entire study area also demonstrate that the MISR LAI has a good relationship with MODIS SR (see Section IV-B). The errors in the LAI estimation were calculated to further illustrate this relationship. The root-mean-square error (RMSE) of the expanded LAI relative to the original MISR LAI is concentrated around 0.1, with the mean RMSE being 0.74 over vegetated area. The close relationships between the MISR LAI and MODIS SR demonstrate the applicability of the proposed algorithm, which expands the MISR LAI using the MODIS reflectance data.

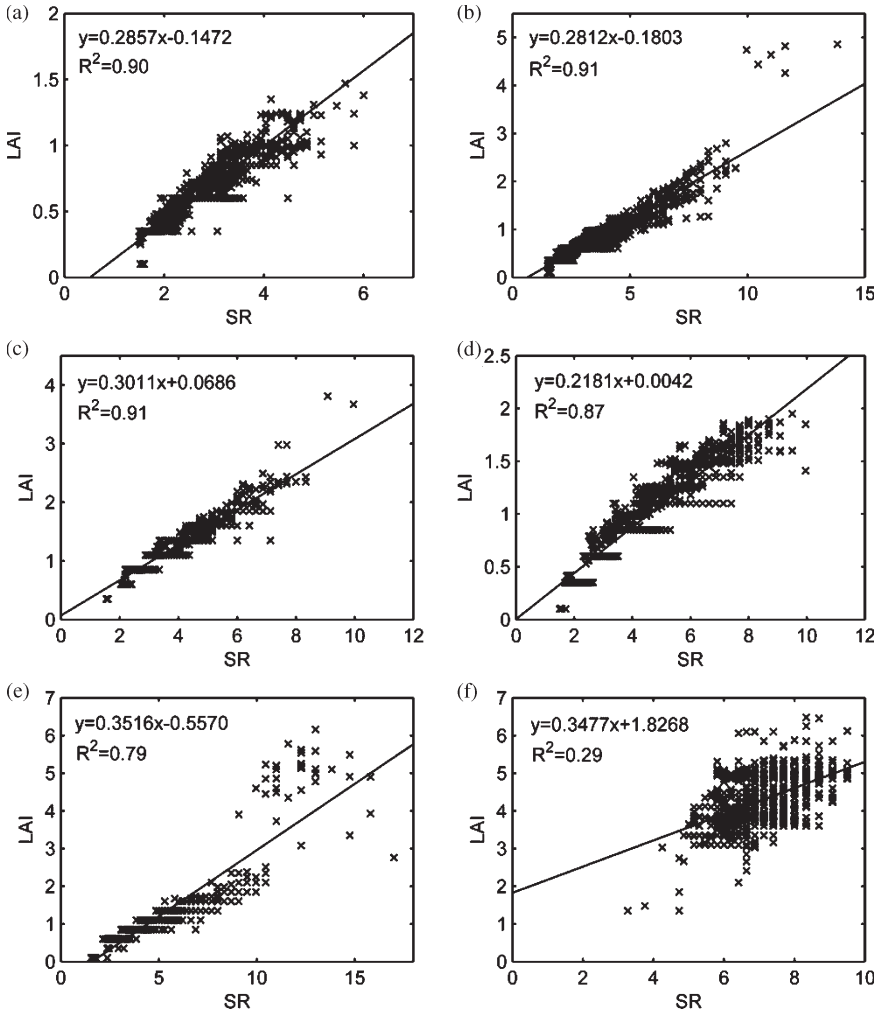

Fig. 1. Plots of MODIS SR and MISR LAI over several sites. (a) Xilingele grassland site (Lat = 44.13° N, Lon = 116.32° E). (b) Jiaozhou cropland site (Lat = 36.12° N, Lon = 119.72° E). (c) Horqin Left Middle Banner shrubland site (Lat = 43.78° N, Lon = 122.35° E). (d) Buerjin broadleaf cropland site (Lat = 47.81° N, Lon = 87.20° E). (e) Xishuangbanna broadleaf forest site (Lat = 21.95° N, Lon = 101.02° E). (f) Daxinganlin needleleaf forest (Lat = 49.47° N, Lon = 70.18° E).

B. Implementation of the MISR LAI Expanding Algorithm

The MISR LAI expanding algorithm consists of three steps. First, MOD09GA, the MISR LAI, and MISR BRF model parameters from 2000 to 2008 are preprocessed. The pixel-level SR-LAI and SR-BRDF relationships are then established from the MISR LAI, BRF model parameters, and MODIS SR. Finally, the expanded LAI is estimated from the MODIS SR with BRDF normalization.

1) Data Preprocessing: The MISR and MODIS data sets, including the MISR LAI, BRF model parameters, MOD09GA\MOD09A1 and MOD15A2 from 2000 to 2008, were first preprocessed to the Albers equal-area projection at 1 km × 1 km spatial resolution through nearest-neighbor interpolation. Reprojected data with the same temporal period were composed to cover the entire mainland of China. The land surface reflectance was then screened for cloud contamination, water, and snow/ice on the basis of the MOD09 state flag.

2) Establishment of the Pixel-Level SR-BRDF and SR-LAI Relationships: Both MISR and MODIS instruments are on-board the Terra satellite with a Sun-synchronous orbit of 16 days. This means that the platform returns to the same location and makes observations under nearly identical angular conditions after 16 days. Fig. 2 is one swath acquired by MISR and MODIS over China on day of year (DOY) 190, 2008. The narrow swath area of the MISR is entirely covered by the MODIS measurements. Therefore, the atmospheric and land surface conditions are nearly the same when the two

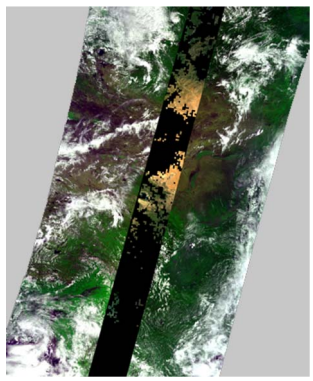

Fig. 2. MISR and MODIS natural color images for DOY 190, 2008. The black stripe is the MISR image.

sensors observe the same ground target. That is, the coincident measurements of MODIS reflectance should be valid as long as there is a valid MISR LAI value for the corresponding location. Although the overlapping region is only a small part for one orbit, the coincident observations of both instruments can cover the entire earth surface over a long period. Thus, the pixel-based MODIS SR-MISR LAI relationship can be established from these two data sets.

The LAI is not complete linearly related with SR. To alleviate the bias from this nonlinearity, the SR-LAI relationship is established for several SR bins. In this paper, SR is divided into ten bins according to the ten equally sized NDVI bins ranging from 0 to 1.0 at an interval of 0.1. The corresponding SR bins are [0, 1.22), [1.22, 1.5), [1.5, 1.86), [1.86, 2.33), [2.33, 3), [3, 4), [4, 5.67), [5.67, 9), [9, 19), [19, $+\infty$). The SR-LAI relationship is assumed linear in each SR bin. The pixel-by-pixel SR-LAI relationships were established from the averages of the long-term normalized MISR LAI for median SR in the 10 SR bins.

The SR should be eliminated the BRDF effects for LAI retrieval. MODIS provides the nadir BRDF-adjusted reflectance product and BRDF model parameters product by inverting the model with observations measured over 16-day periods with the assumption that vegetation status is stable during the 16-day composite period. However, the vegetation changes rapidly at the beginning and the end of the growing season. Additionally, it is generally difficult to acquire the required number of clear-sky observations for implementing its main algorithm, resulting in a large number of filled values or low-quality retrievals obtained from the back-up algorithm in MOD43 products. The MISR with nine angular observations is an ideal tool for BRDF parameter retrieval. MISR provides daily BRF model parameters products using the modified Rahman model [13], [17]. In establishing SR-LAI relationships, the MODIS directional reflectance could be normalized to nadir geometry using corresponding MISR BRF model parameters. However, in LAI retrieval, daily MISR BRF model parameter products cannot cover the entire MODIS swath. The BRDF properties should be similar for those pixels with the same land-cover type and similar biophysical conditions [26]. Thus, the shape of the BRDF is similar at the same site if the land-cover type does not change largely. Here, the vegetation biophysical condition is described by SR. The pixel-based SR-LAI and SR-BRDF relationships are established from MISR LAI, BRF model parameters, and the coincident MODIS reflectance as follows:

Step 1) The LAI, BRF model parameters, and reflectance are matched in pairs. The LAI/BRF model parameters—reflectance pairs for each pixel are generated from the MISR LAI, BRF model parameters, and MOD09GA surface reflectances for 2000–2008. First, the MISR product files are matched with the MOD09GA file acquired on the same day. For each pixel, the valid MISR LAI and BRF model parameters during 2000–2008 are then matched with the most spatially proximal MODIS daily land surface reflectance in the red and near-infrared bands acquired on the same day to construct the LAI, BRF model parameters, and reflectance pairs.

Step 2) SR-LAI and SR-BRF model parameter data pairs are generated. For each LAI, BRF model parameters, and reflectance pair of a pixel, the red and near-infrared band reflectances of MODIS are normalized to a common geometry—the nadir view, 45° solar zenith angle (SZA) and 0° relative azimuth angle (RAA)—using the modified Rahman model and BRF model parameters of the data pair. The BRF model describes the BRDF properties of the land surface using three free parameters (r_0, k, b) with consideration of the hotspot effect [13], [17].

Given an observation with view geometry $(-\mu, \mu_0, \phi - \phi_0)$, the directional reflectance can be simulated using three free parameters (r_0, k, b), where μ and μ_0 are the cosine of the viewing and SZAs of the observations, which are defined with respect to the normal to the surface ellipsoid, ϕ is the view azimuth angle, and ϕ_0 is the solar azimuth angle. Using the r_0, k, b data sets taken from the MISR BRF model parameter product, the observed MODIS directional reflectance $R_{obs}(SZA_{obs}, VZA_{obs}, RAA_{obs})$ at a SZA, viewing zenith angle (VZA) and RAA of $SZA_{obs}, VZA_{obs}, RAA_{obs}$ is normalized to $R(45°, 0°, 0°)$ with common geometry of SZA $=$ 45°, VZA $= 0°$ and RAA $= 0°$

$$R(45°,0°,0°) = \frac{R(-\cos(0°), \cos(45°), 0°)}{R(-\cos(VZA_{obs}), \cos(SZA_{obs}), RAA_{obs})} \times R_{obs}(SZA_{obs}, VZA_{obs}, RAA_{obs}) \quad (1)$$

where $R(-\cos(0°), \cos(45°), 0°)$ and $R(-\cos(VZA_{obs}), \cos(SZA_{obs}), RAA_{obs})$ are the reflectance simulated using the Rahman model with viewing geometry SZA $= 45°$, VZA $= 0°$ and RAA $= 0°$ and observation geometry of a pixel SZA $= SZA_{obs}$, VZA $= VZA_{obs}$ and RAA $= RAA_{obs}$.

SR is calculated using the BRDF-normalized MODIS red (ρ_{Red}) and near-infrared band (ρ_{Nir}) land surface reflectance $(SR = \rho_{Nir}/\rho_{\mathrm{Red}})$. SR-LAI and SR-BRF model parameter data pairs are then determined for each pixel using the BRDF-normalized SR.

Step 3) Pixel-level SR-LAI and SR-BRDF relationships are established. For each pixel, the SR-LAI and SR-BRF model parameter pairs are divided into ten bins according to SR ranges of [0, 1.22), [1.22, 1.5), [1.5, 1.86), [1.86, 2.33), [2.33, 3), [3, 4), [4, 5.67), [5.67, 9), [9, 19), [19, $+\infty$). The LAI and BRF model parameters in the SR-LAI and SR-BRF model parameter pairs are normalized to the median SR value for each bin through linear interpolation. The mean LAI and BRF model parameters corresponding to the median SR of each SR bin are calculated according to the interpolated LAI and BRF model parameters.

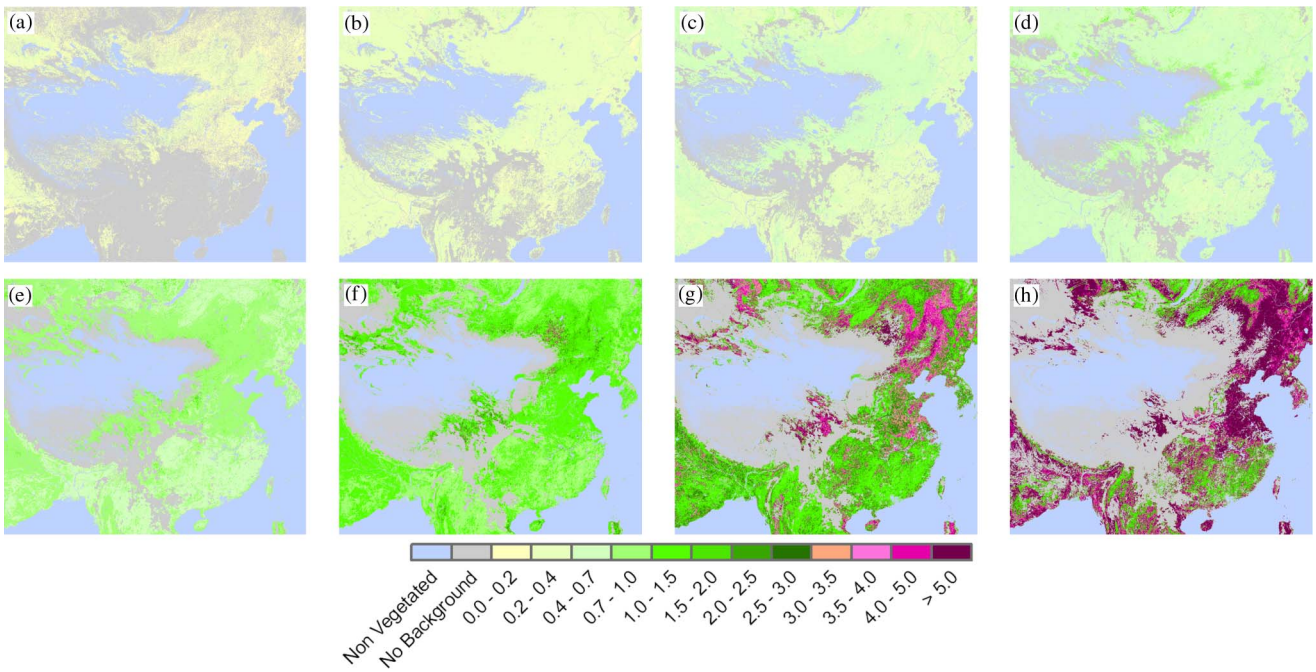

Fig. 3. Pixel-based SR-LAI relationships. SR range (a) [1.22, 1.5); (b) [1.5, 1.86); (c) [1.86, 2.33); (d) [2.33, 3); (e) [3, 4); (f) [4, 5.67); (g) [5.67, 9); (h) [9, 19).

Step 4) The SR-LAI and SR-BRDF relationship data sets, which are represented by the mean LAI and BRF model parameters for the 10 SR bins, are saved. The output for pixel-level SR-LAI relationships contains ten layers of mean LAI maps for the ten SR bins. For the SR-BRDF relationships, there are totally 60 layers of mean BRF model parameters for the ten SR bins—three layers for the red band and three layers for the near-infrared band in each SR bin. Fig. 3 shows the spatial distribution of the LAI corresponding to eight SR bins from 1.22 to 19. Because the pixels with SR less than 1.22 are considered as nonvegetated and there are only a few pixels with SR larger than 19, the maps for SR < 1.22 and SR ≥ 19 are not shown here. There are a few pixels without valid values in Fig. 3, mainly in southwestern China and northern Vietnam. This means that there are no sufficient valid MISR LAIs for these pixels during 2000–2008.

3) LAI Retrieval Using Land Surface Reflectance: After pixel-level SR-LAI and SR-BRDF relationships are established, the expanded LAI can be retrieved from MODIS land surface reflectance observations. First, MODIS reflectance in the red and near-infrared bands is BRDF normalized using the modified Rahman model and above pixel-level SR-BRDF relationships. For each pixel, the first guess of SR is made using MODIS reflectance in the red and near-infrared bands. With this SR value, three BRF model parameters are determined for each band according to SR-BRDF relationships for that pixel. Employing these matched BRF model parameters and the modified Rahman model, land surface reflectance in red and near-infrared bands is normalized to a standard geometry (i.e., the nadir view, 45° SZA and 0° RAA) using formula (1) and further used to calculate SR. After BRDF normalization, LAI inversion is conducted as follows. For each pixel in the SR image, the LAI values in the two adjacent SR bins of this pixel are obtained from the SR-LAI relationship maps (Fig. 3). If LAI values of these two SR-LAI relationship maps are both valid, the retrieved LAI is determined through linear interpolation. If only one LAI value of the SR-LAI relationship maps is valid, the retrieved LAI is assumed to be this LAI value. When the two LAI values in the SR-LAI relationship maps are both invalid, the LAI retrieval fails and the pixel is labeled as no background. The pixels with SR less than 1.22 are labeled as nonvegetated, and the retrieval is not carried out.

C. Estimation of the Retrieval Index

The retrieval index (RI) is defined as the ratio of the total number of pixels (NP_{Retr}) which LAI has been effectively retrieved to the total number of pixels (NP_{total}) which LAI should be retrieved in a region during a period (Formula 2). It is an indicator for evaluating the time coverage and retrieval capability of MISR LAI, MODIS LAI and the expanded LAI with daily and 8-day composite data sets. The higher RI means that more valid LAI values are retrieved by the algorithm from the sensor data

$$RI = \frac{NP_{\mathrm{Retr}}}{NP_{total}}. \tag{2}$$

Since the LAI algorithm is expected to perform for the vegetated pixels, the RI is only calculated for the vegetated pixels. MODIS land cover type product MCD12Q1 is used to exclude the nonvegetated pixels. Additionally, the nonvegetated pixels were excluded in the MISR LAI algorithm using the criterion of NDVI ≤ 0.2, only those pixels with NDVI > 0.2 are assumed as vegetated and counted in RI calculation.

The NP_{Retr} is calculated by counting all the pixels with valid LAI retrieval. All the vegetated pixels in MOD12 with NDVI > 0.2 should be implemented for LAI retrieval, and their total number is the NP_{total}. The NDVI time series calculated from MODIS MOD09 reflectance data are used to infer the NP_{total}. Although a cloud flag is provided in this product, it is unable to identify directly whether a pixel is vegetated (with NDVI > 0.2 assuming no cloud contamination) or nonvegetated from these reflectance data because some pixels were screened by the cloud. Cloud and other noises should be removed from these reflectance data before counting the NP_{total}. In this paper, the interpolation method by Lu *et al.* [27] was used to remove clouds and other noise of time series of the NDVI data set from MODIS 8-day composite land-surface reflectance product MOD09A1. The interpolated NDVI from the MOD09 data is used as an indicator for land surface vegetation. Those pixels labeled as vegetated in MOD12 and with NDVI > 0.2 in the interpolated NDVI data set were then counted as the total processed pixels, NP_{total}, and were used for calculating the RI for 8-day composite MODIS, MISR and the new LAI data sets. The number was multiplied by 8 when evaluating the RI for the daily tile LAI data sets.

D. Estimation of Noise

To quantify the temporal continuity of the LAI data sets, the noise of MODIS and derived LAI time series is estimated as [28]

$$Noise(y) = \sqrt{\frac{\sum_{i=1}^{N-2}\left(y_{i+1} - \frac{y_{i+2}-y_i}{day_{i+2}-day_i}(day_{i+1}-day_i) - y_i\right)^2}{N-2}} \quad (3)$$

where N is the total number of valid LAI values, i refers to a specific LAI in the time series data set, $y_{\mathrm{i+1}}$ and y_{i} are the $(i+1)$th and ith LAIs, respectively, and $\mathrm{day}_{\mathrm{i+1}}$ and $\mathrm{day}_{\mathrm{i}}$ are the day numbers corresponding to the $(i+1)$th and ith LAIs, respectively.

The noise for each pixel is calculated from the time series MOD15A2 LAI and the expanded LAI according to four criteria. 1) Only those MODIS LAIs generated from the main algorithm are used. 2) Both MOD15A2 and the expanded LAI are valid on the same day. 3) The noise is assumed a linear variation between two dates. This linear-variation hypothesis is valid only when the period is short [28]. Therefore, the noise is computed when LAIs are valid for three continuous 8-day composite periods. 4) To avoid the effects of outliers, the 5% of the triplets having the largest biases in LAI which result in large values of the numerator in formula 3 are discarded.

IV. Results and Validation

A. Results

Fig. 4 is an expanded LAI map dated July 12–19, 2008. The spatial pattern of the expanded LAI on this map is consistent with the vegetation distribution in China. The LAI has a concentration of high values from 4 to 6 in the Xing'an mountainous region, where mature forests are the dominant vegetation. The LAI of dense crops, grasses, and forests distributed in northern and southern China is also high. Large nonvegetated areas in northwestern China are easily distinguished, with the LAI being close to zero. LAI values for some pixels are invalid in Tibet, northwestern Sichuan, southern Shanxi, central Yunnan, Taiwan, and northern Vietnam as a result of invalid SR-LAI relationships, where the MISR LAI algorithm failed to retrieve the LAI for the period from 2000 to 2008.

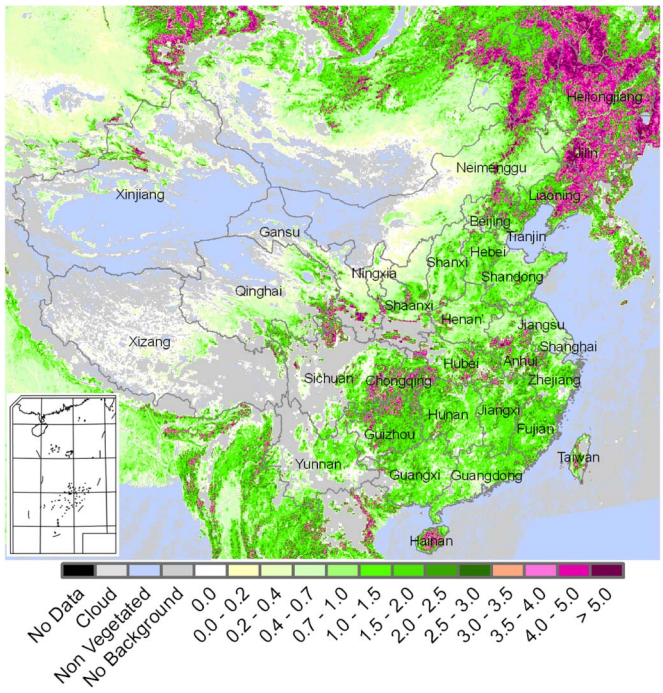

Fig. 4. Expanded LAI map of China for July 12–19, 2008.

B. Comparison With Existing MISR LAI Products

The 8-day MISR LAI was obtained from the daily MISR standard LAI product for 2000–2008 by employing the maximum NDVI composite method, and then compared with the 8-day expanded LAI from MOD09A1. Fig. 5(a) shows the distribution of the RMSE of the expanded LAI relative to the MISR LAI. The RMSE of most pixels is less than 1, while the RMSE is larger with values from 1 to 2 for Changbaishan and the Xing'an Mountains in northeastern China as a result of high LAI values in these regions. Fig. 5(b) shows a histogram of the LAI RMSE. The RMSE is mainly around 0.1. The RMSE is less than 1 for 81% pixels with mean RMSE of 0.74 of the vegetated pixels, and this percentage increases to 99.6% for RMSE of less than 2.

C. Time Coverage Evaluation

1) Comparison of RI for Daily LAI Products: The daily expanded LAI from 2000 to 2008 was retrieved from MOD09GA reflectance. The RIs of the expanded LAI over four tiles that cover the main vegetated region of China—H26V04, H27V05,

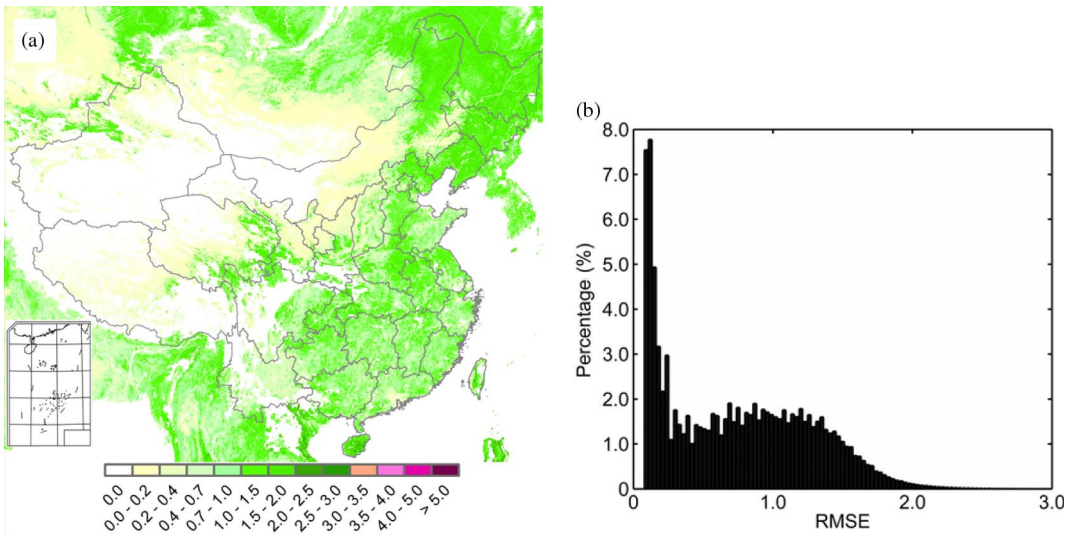

Fig. 5. Error analysis of the original and the expanded LAI products over China. (a) RMSE map. (b) RMSE histogram.

TABLE I
RIS OF THE DAILY MISR LAI AND EXPANDED LAI IN FOUR TILES COVERING THE MAIN VEGETATED REGIONS IN CHINA

Tile	H26V04	H27V05	H27V06	H28V06
MISR LAI RI (%)	2.8	2.1	1.0	1.4
The expanded LAI RI (%)	38.6	25.3	18.2	22.8

H27V06, and H28V06—were mapped. MISR RIs in the corresponding tiles were also calculated from MISR daily LAI products for 2000–2008. Table I shows the RIs for vegetated pixels. The RIs of MISR LAI products are around 1.8%, which means that the valid daily MISR LAI is only available for 1.8% of vegetated areas in China. With the integration of MODIS observations, the percentage increases to about 26.2%. RIs of the two data sets are high in tile H26V04, which corresponds to northeastern China, where rainfall events are less frequent and cloud screening is not significant. In contrast, the RIs of tiles H27V06 and H28V06 are obviously lower for the two LAI data sets, probably owing to there being fewer pixels with valid MISR LAI and MODIS reflectance because of heavy cloud contamination. In addition, the MISR LAI is missed in the southeastern part of tile H27V06, resulting in the failure of the expanding LAI algorithm in this region.

2) Comparison of the RI for the 8-day Composite LAI Over China: RIs were mapped for the 8-day composite MISR LAI, MOD15A2 LAI, and expanded LAI generated from MOD9A1 from 2000 to 2008 (Fig. 6). The RI of the MODIS LAI product (MOD15A2) is more than 60% in most vegetated areas. The snow and ice cover in the northern/northeastern part and the rainy/cloudy days in southwestern China and Southeast Asia may result in frequent failures of the MODIS main algorithm. The backup algorithm is then used to estimate the LAI. Thus, the RI of the MODIS LAI obtained with the main algorithm is low in these regions [Fig. 6(b)]. The RI of the MISR LAI is much less than that of MODIS and is about 30–50% in India, eastern Kazakhstan and northern Mongolia and below 30% in other regions. In the northern part of the study area and southwestern China and on the Tibet Plateau, the RI values of the

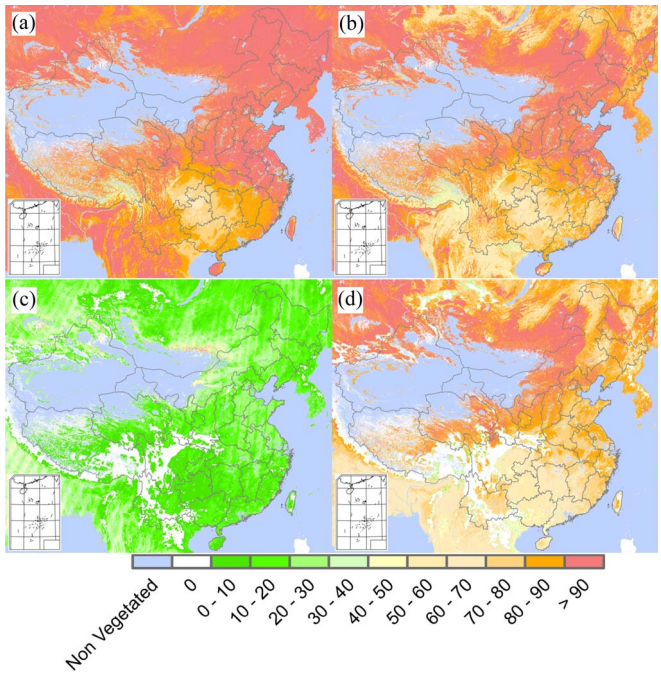

Fig. 6. Retrieval index maps (unit: %) of the 8-day composite MODIS LAI, the MISR LAI and the expanded LAI products from 2000 to 2008 for China. (a) RI map for the MOD15A2 LAI. (b) RI map for the MOD15A2 from main algorithm LAI. (c) RI map for the MISR LAI; d) RI map for the expanded LAI.

MISR LAI are even below 10%, indicating the discontinuity of the MISR LAI product. The RI of the expanded LAI increases to more than 50% in most of the vegetated areas.

For all the vegetated pixels over the study area, the RI for MOD15A2 is 90.7%, and that for the LAI generated from the main algorithms remains above 80%. The RI of the MISR LAI is only 15.5%, indicating that no valid MISR LAI is available for more than 80% of vegetated areas even after 8-day compositing. Such low coverage of MISR LAI products would definitely inhibit their practical usefulness. The RI of the expanded LAI increases to 65.2%, which means that valid LAI is provided for 65% of vegetated areas every 8 days.

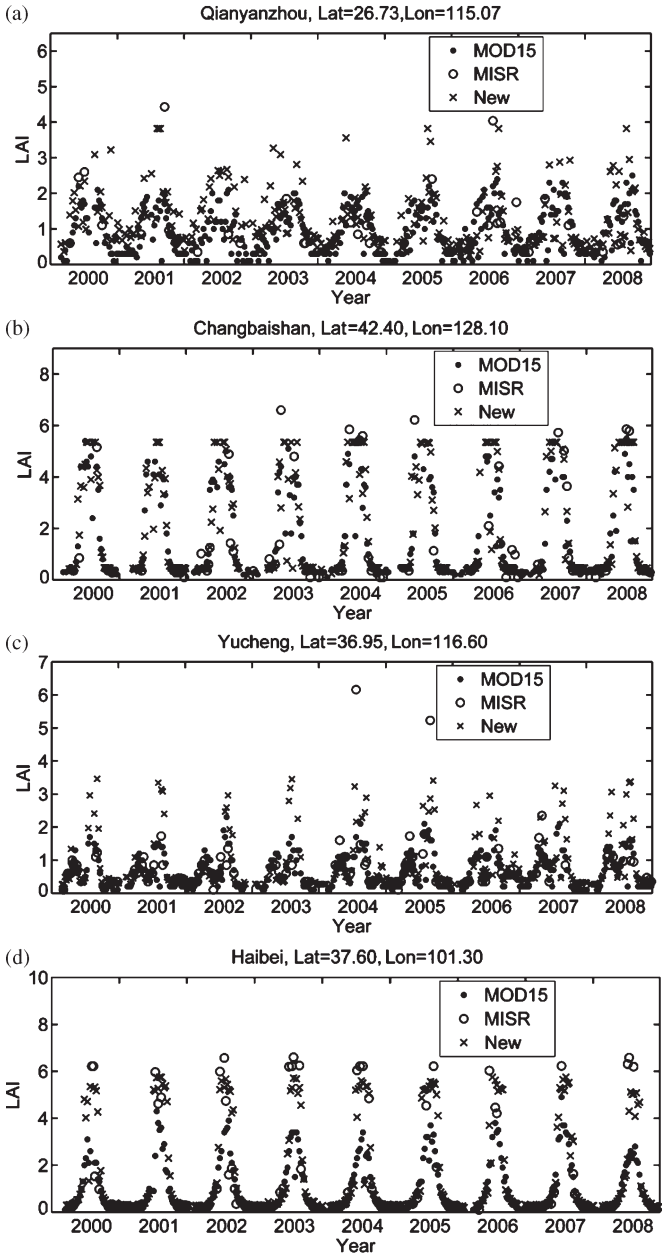

Fig. 7. Temporal profiles of the MODIS LAI, MISR LAI and the expanded LAI over several Fluxnet sites. (a) Qianyanzhou. (b) Changbaishan. (c) Yucheng. (d) Haibei.

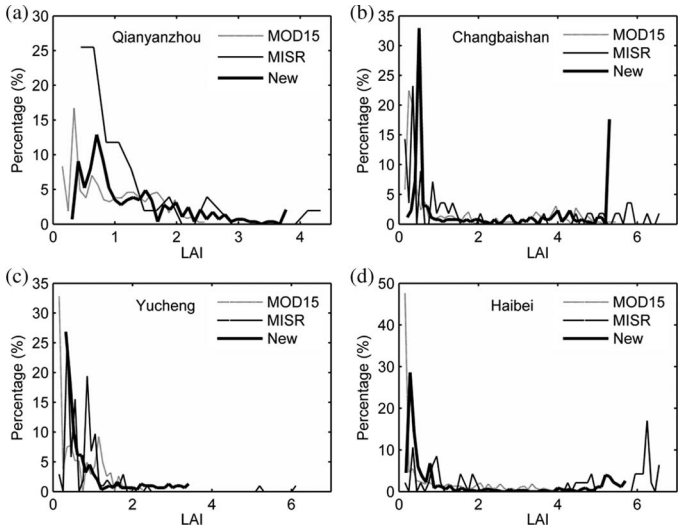

Fig. 8. Histogram of the MODIS LAI, MISR LAI and the expanded LAI over several Fluxnet sites. (a) Qianyanzhou. (b) Changbaishan. (c) Yucheng. (d) Haibei.

D. Evaluation of Temporal Consistency

1) Temporal Profiles of the LAI at Typical Sites: To further evaluate the performance of the expanding algorithm in terms of temporal consistency and the seasonal and interannual variations, temporal profiles of the 8-day composite MISR LAI, MODIS LAI generate from the main algorithm, and the expanded LAI were compared over several typical Fluxnet sites in China, namely the Qianyanzhou coniferous forest site, the Changbaishan mixed forest site, the Yucheng cropland (winter wheat and summer maize rotation) site, and the Haibei grassland site.

The temporal profiles of the three LAI data sets over the four Fluxnet sites are presented in Fig. 7. The number of valid MISR LAIs is less than 12 per year, which makes it too sparse to fully characterize the seasonal and interannual dynamics of the vegetation at all four sites. The number of valid LAI increased significantly to about 33 per year for the expanded LAI. Fig. 8 shows the histograms of the three LAI data sets. The MISR LAI values are close to MODIS data with a mean LAI difference of 0.20 at the Qianyanzhou, Changbaishan, and Yucheng sites. At the Haibei site, the MISR and expanded LAI are larger than MOD15A2 LAI. The expanded LAI could represent the seasonal variations of the LAI over all sites, including the LAI seasonal variations of the winter wheat-summer maize rotation system at the Yucheng site. Although the MODIS LAI represents the dynamics of local vegetation, there are still outliers in the temporal profiles in spite of only using the results generated from the main algorithm, particularly for the Qianyanzhou and Changbaishan forest sites. At the Yucheng cropland site, outliers with LAI larger than 5 are also presented in original MISR LAI products. There are fewer outliers in the expanded LAI series than in the MODIS LAI series. This is probably due to the low sensitivity of SR to atmospheric contamination and other noise [29]. At the Changbaishan site [Fig. 8(b)], the SR is greater than 19 (NDVI > 0.9) in mid-summer due to the dense forest. However, the valid retrievals in existing MISR LAI products are too sparse to generate pixel-level SR-LAI for SR bin of [19, $+\infty$). Thus, the retrieved LAI with SR greater than 19 in mid-summer used the knowledge LAI value for SR bin of [9, 19) for this pixel, resulting high frequency of LAI around 5. Although this may underestimate LAI of dense forest, the large uncertainties from extrapolation could be avoided.

2) Temporal Noise in the MODIS and the Expanded LAIs: Noise maps are produced from the 8-day composite MOD15A2 and the expanded LAI for 2000 to 2008. The noise was not calculated for the MISR LAI products owing to the limited number of valid pixels. The average noise of the two data sets was computed for vegetated pixels. Only the pixels with valid noise estimation for both the MODIS and the expanded LAI

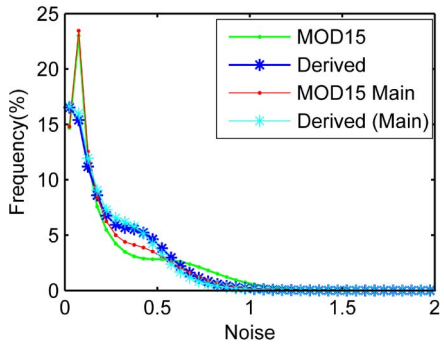

Fig. 9. Histograms of the noise of MODIS and the expanded LAI, including results of the MOD15A2 main algorithm (MOD15 Main, red line), the expanded LAI for days when the MODIS main algorithm is employed (Derived (Main), bright blue), MOD15A2 using both the main and backup algorithms (MOD15, green line), and the expanded LAI for the corresponding days (Derived, blue line).

products were included in the statistical analysis. In MODIS LAI algorithm, the back-up algorithm is employed when the main algorithm fails to work which is mainly due to the low-quality reflectance data inputs being contaminated by clouds or other noise [3]. In order to evaluate the robustness of the expanding algorithm to the low-quality inputs, both the main algorithm and back-up algorithm are represented in RI calculation.

The noise is similar for the MODIS LAI generated from the main algorithm (0.234) and the expanded LAI for the same pixels (0.238). When those pixels which MODIS LAI is generated from the backup algorithm are considered, that is, the LAI derived from low-quality reflectance data are included in RI calculation, the noise for the MODIS LAI generated from both main and backup algorithms increases by 18.38% (from 0.234 to 0.277), while the noise of the expanded LAI for the same pixels only increases by 7% (from 0.238 to 0.255). Fig. 9 is a histogram of the noise for the MODIS LAI and the expanded LAI. When the pixels treated with the back-up algorithm are included, the noise for MODIS LAI increases from 0.6 to 1.0 (Fig. 9). In contrast, this variation is not significant for the expanded LAI, indicating that the expanded LAI is more robust to cloud contamination and other noise of inputs. This robustness of the MISR LAI expanding algorithm is mainly due to the less sensitivity of SR to atmospheric contamination and other noise [29].

E. Validation of the Expanded LAI at the Regional Scale

The expanded LAI is compared with field measurements in Baohe, Maoershan, and Hulunbeier regions to validate the expanding algorithm. It is usually difficult to acquire clear-sky satellite imagery coincident with field LAI measurements. In this comparison, the clear-sky TM images, which are temporally closest to the field measurements, are used to generate high-resolution maps by developing an empirical relationship between the field measurements and corresponding VI pixels derived from the TM scene, which is critical in upscaling *in situ* measurements [30]. Although the dates of Landsat TM and field measurement may not be the same, since the validations are usually performed during the period when vegetation is relative stable, this difference of date only affects the parameters of the regression model, and its influence on the comparison result is negligible.

1) Validation of the Expanded LAI in the Baohe Region: The Baohe site is located on the southwestern slope of Taibaishan Natural Reserve in the middle of the Qinling Mountains ($31°42'$N–$39°35'$N, $105°29'$E–$110°15'$E). Its elevation ranges from 510 to 3767 m above sea level, and the vegetation type and density vary with the terrain aspect and elevation. The dominant vegetation type is pine and broadleaf mixed forest as well as broadleaf forest. The LAI was measured in nine sampling plots with area of about 30 m $\times$ 30 m using a TRAC instrument with consideration of foliage clumping in early June 2004. A fine-resolution LAI map with 30-m resolution was produced from two Landsat TM images acquired on June 5, 2003 using the empirical TM VI and field LAI relationships ($\mathrm{LAI} = 5.6974\mathrm{NDVI} - 0.1986$ for mixed forest, and $\mathrm{LAI} = 5.9709\mathrm{NDVI} - 0.8423$ for broadleaf forest) [31].

The expanded LAI map with 500 m resolution was produced from MOD09A1 land surface reflectance obtained on DOY 153–160 (June 2–9) in 2004 in Baohe. The two LAI maps were transformed to the Albers equal area projection and aggregated to 500 m $\times$ 500 m resolution by averaging valid LAI values in 500 m $\times$ 500 m blocks. Fig. 10(a) and (b) show the TM and expanded LAI map, respectively. The TM LAI and the expanded LAI are low (less than 1.5) in northern and southwestern part of the experimental area. In the middle and central southern parts, both the TM LAI and the expanded LAI are much higher (around 5.0). The expanded LAI is missing in northwestern and southeastern parts of the experimental area due to the invalid SR-LAI relationships on such rugged terrain in the Qinling Mountains [Fig. 10(b)]. In pixel-by-pixel comparison of the TM LAI with the expanded LAI [Fig. 10(c)], the R^2 and RMSE are 0.32 and 1.48, respectively. The mean values of the TM LAI map (3.82) and retrieved LAI map (3.09) differ by 0.73. Using Landsat LAI images as the standard, the expanded LAI underestimates field measurements by about 19.1%.

2) Validation of the Expanded LAI in the Maoershan Region: The Maoershan site is located in Heilongjiang province, where the main vegetation cover is larch and broadleaf mixed forest. Effective LAI measurements were performed in 23 sampling plots of 50 m $\times$ 50 m with a LAI 2000 instrument on July 12–18, 2009. Additionally, the clumping index was also measured with a TRAC instrument over the sampling plots. Landsat TM imagery acquired on June 24, 2009 was georeferenced. The radiance was converted to spectral reflectance to calculate the reduced SR (RSR), and then used to establish the empirical relationship with the field effective LAI measurements ($\mathrm{LAI_{eff}} = 0.4939\mathrm{RSR} + 0.5185$). A fine-resolution (30 m) effective LAI map was generated on the basis of this relationship. The vegetated pixels in TM imagery were classified to be coniferous forests, broadleaf forests, and mixed forests. The effective LAI was then converted to the true LAI with the average value of field-measured clumping index (Ω) for each biome type ($\mathrm{LAI} = \mathrm{LAI_{eff}}/\Omega$), which are 0.63 for coniferous forests, 0.83 for broadleaf forests, and 0.75 for mixed forests [32].

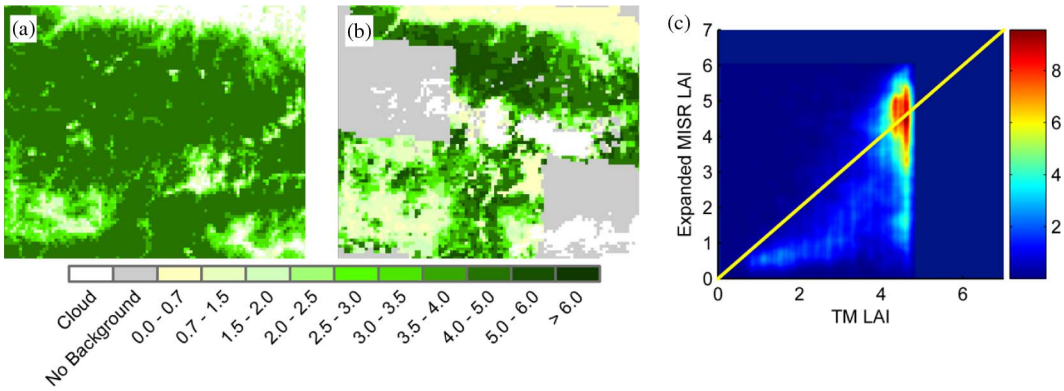

Fig. 10. Validation of the LAI in Baohe. (a) TM LAI on DOY 156, 2003. (b) the expanded LAI. (c) TM LAI versus the expanded LAI, $y = 0.9019x - 0.3552$.

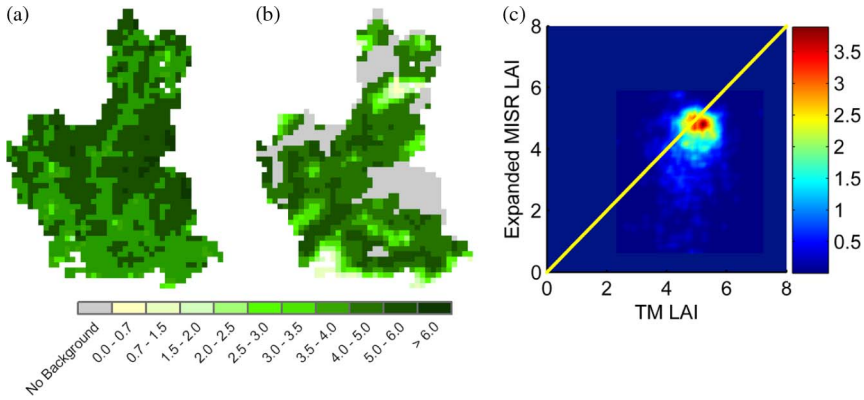

Fig. 11. Validation of the LAI in Maoershan. (a) TM LAI on DOY 175, 2009. (b) The expanded LAI. (c) TM LAI versus the expanded LAI, $y = 0.3309x + 2.6083$.

The expanded LAI was also derived from MOD09GA land surface reflectance acquired on DOY 175 (June 24) in 2009. The TM and the expanded LAI maps were transformed to the Albers equal area projection and aggregated to 500 m $\times$ 500 m resolution. As this site is also located in the Maoershan Mountains, the expanded LAI is not retrieved owing to the missing SR-LAI relationship for northwestern and central eastern regions. The comparison is shown in Fig. 11. The difference between the mean TM LAI (4.92) and the derived mean LAI (4.24) is 0.68. The expanded LAI underestimates field measurements by about 13.8% using TM LAI images as the standard. In the pixel-by-pixel comparison between these two LAI maps in Fig. 11(c), R^2 and RMSE are 0.04 and 1.2, respectively.

3) Validation of the Expanded LAI in the Hulunbeier Region: The Hulunbeier site is located at the Hulunbeier grassland ecosystem national field site in Inner Mongolia province ($49°20'\mathrm{N}, 119°59'\mathrm{E}$). The main vegetation cover is temperate meadow steppe, and the dominant species are Leymus chinensis, Stipa baicalensis, and Poa sphonbylodes. On June 21–26, 2010, LAI measurements were performed in 52 sampling plots of 50 m $\times$ 50 m using a LAI-2000 instrument. The true LAI is calculated from the field-measured effective LAI with the assumption that the clumping index is 1.0 for this grassland region. Landsat TM imagery (path: 123, row: 26) acquired on June 21, 2010 was used to derive a high-resolution LAI map. After georeferencing, radiation correction, and atmospheric correction, the TM radiance was converted to spectral reflectance to calculate VI RSR. As the *in situ* LAI is the mean value of the sample plots of 50 m $\times$ 50 m, the RSR was calculated from the mean reflectance of 3 $\times$ 3 pixels around the sample site, and its relationship with the field LAI measurements, $LAI = 0.232 \times RSR^{1.458}$, was established. A fine-resolution (30 m) LAI map was then generated on the basis of this relationship.

The expanded LAI map was also produced from MOD09GA land surface reflectance acquired on DOY 175 (June 24) in 2010. The two LAI maps were transformed to the Albers equal area projection and aggregated to 500 m $\times$ 500 m resolution. Fig. 12 presents the comparison of the TM LAI and the expanded LAI. The LAI is low (around 0.5) in the southwestern region of the experimental area and similar to the TM LAI (around 0.3). Meanwhile, the expanded LAI and TM results are both higher (around 2.0) in northwest and eastern parts of the image. The expanded LAI also captures the dense vegetation in the northeastern area, with the LAI exceeding 3. There was no failed inversion at the Hulunbeier site owing to its flat terrain. The mean values of the TM LAI (1.42) and the derived LAI (1.44) differ by about 0.02. Pixel-by-pixel comparison [Fig. 12(c)] shows that the R^2 and RMSE value of the two LAI

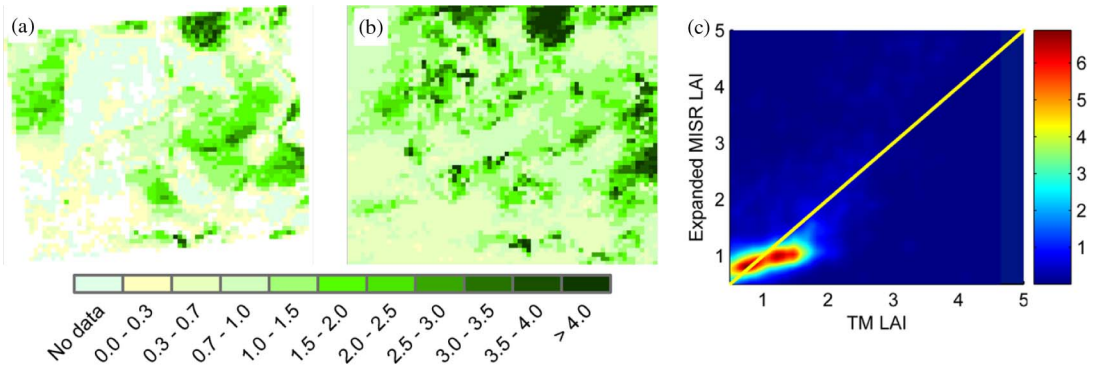

Fig. 12. Validation of the LAI in Hulunbeier. (a) TM LAI on DOY 172, 2010. (b) The expanded LAI. (c) TM LAI versus the expanded LAI, $y = 0.939x + 0.1073$.

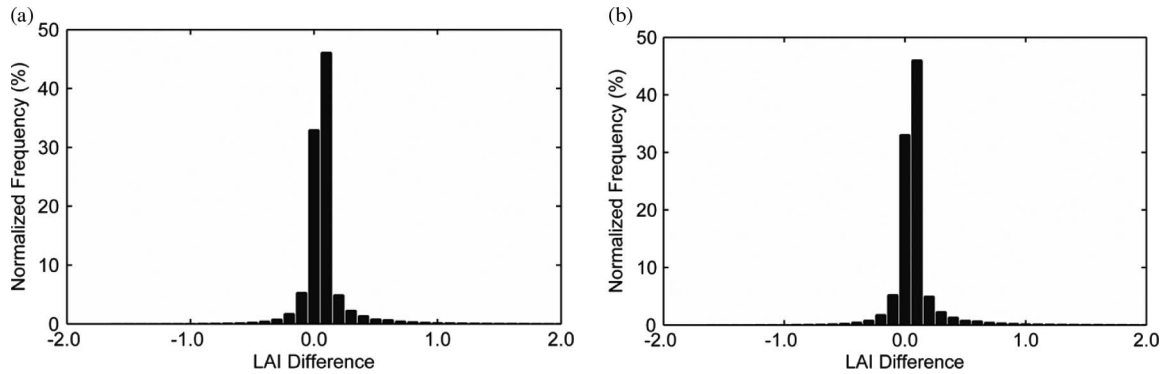

Fig. 13. LAI difference with and without BRDF normalization in (a) 2007 and (b) 2008.

maps are 0.53 and 0.62, respectively. Using TM LAI map as the standard, the expanded LAI overestimates field measurements by about 1.4%.

F. BRDF Effects on the Derived LAI

The BRDF effect is another factor affecting LAI retrieval based on directional land surface reflectance. The MISR BRF model parameter products in the expanding algorithm are used to minimize the BRDF effect. The quality of this BRDF data set may affect the accuracy of the LAI retrieval. To better understand how much variation in the observational geometry leads to uncertainty in the LAI retrieval, the LAIs are derived from MOD09A1 reflectance for 2007 and 2008 with and without BRDF normalization using the MISR LAI expanding algorithm. And a comparison is then made pixel by pixel (Fig. 13).

It is found that the effects of the BRDF are not significant for LAI retrieval from MODIS data. This suggests that, to simplify the algorithms and to improve the computation efficiency, BRDF normalization can be ignored in expanding LAI with MODIS data. This differs a little from the finding of Deng *et al.* [5], who suggested the BRDF effect has a significant influence on LAI retrieval for VEGETATION observations. This is mainly due to the difference in geometric conditions between MODIS and VEGETATION. This BRDF correction procedure increases the theoretical integrity and reasonability of the algorithm. Thus, the BRDF normalization should be included when a more accurate expanded LAI is preferred or the expanding algorithm is applied to other sensors.

V. Discussion

The goal of this paper is to produce an LAI data set with MISR LAI characteristics and high temporal resolution through fusing MODIS observations with MISR data. There are still limitations that affect the performance of the algorithm.

One of the major limitations is the invalid values of SR-LAI relationships. The absence of SR-LAI relationship means that there are no sufficient valid MISR LAIs for these pixels during nine-year period from 2000 to 2008. At-launch MISR LAI retrievals are not performed over topographically rugged terrain or the scene without valid aerosol retrieval [13], which are the main reason for the absence of valid values. Additionally, frequent clouds may result in the failure of the MISR sensor to acquire enough valid observations. The absence of SR-LAI relationship impedes the performance of the algorithm to retrieve LAI. Although the RI has been significantly improved, it is still lower than that of MODIS.

There are discrepancies between the expanded LAI and the original MISR LAI products as well as the field measurements. The expanding algorithm show better performance for grassland, while it shows larger biases for forests. The at-launch MISR LAI product for needleleaf forest remains at a provisional quality level, which may result in biases in the expanded LAI for forests [18]. Additionally, the selected VI, which may not be the optimum related with LAI for forest,

may also introduce some discrepancies. In the current version of the MISR expanding LAI algorithm, SR is selected as a proxy of vegetation state, and the linear relationship between SR and LAI is assumed. However, the SR and LAI may not have strong linear relationship in some regions due to the differences in vegetation species, canopy structure, and soil background. In the analysis of the relationship between the MISR LAI and MODIS SR in Section III-A, the linear relationship is significant for grassland, cereal crops, shrubland, and broadleaf crop, while the relation is not strong for forest, particularly for needleleaf forest, for which the RSR shows a better correlation with the field measurements.

The performance of our algorithm may be improved by employing better LAI data sets generated from MISR observations. If the invalid retrieval of MISR LAI product could be reduced, the spatial and temporal coverage of the expanded MISR LAI could be further increased. Additionally, MISR multi-angle observation is an excellent candidate for mapping of the vegetation structure, such as canopy height, understory reflectance, and clumping index, which are primary parameters for estimating the LAI. Recently, new works on improving LAI retrieval from MISR data have been presented, such as the separation of the contribution of the overstory and understory [15]. The expanded LAI may be improved if better LAI products from the MISR measurements are available to establish pixel-based SR-LAI relationships.

VI. Conclusion

In this paper, we present a new algorithm that expands the MISR LAI product to high temporal resolution through fusing the MISR LAI product with daily MODIS data. Pixel-based SR-LAI relationships were established from the long-term MISR LAI and MODIS land surface reflectance and then used to derive the LAI from MODIS surface reflectance. MISR BRF model parameter products were used to correct the angular variations in MODIS directional surface reflectance.

The new expanded LAI data series was compared with the original MISR and MODIS LAI products for a 9-year period (2000 to 2008) to assess the retrieval capability, temporal consistency, and bias of the expanding algorithm. The results show that the MISR LAI expanding algorithm significantly improves the coverage of the MISR LAI with good temporal consistency and reasonable seasonal dynamics while retaining the merits of the original MISR LAI. The daily RI of the MISR LAI product improves from 1.8% to about 26.2%, and the RI of the 8-day composite increases from 15.5% to 65.2%. The expanded LAI is in good agreement with the original MISR LAI product, with the RMSE less than 1.0 for 81% pixels. The noise in the expanded LAI time series is similar to that in the MODIS LAI product generated from the MODIS main algorithm. The quality of the expanded LAI is less sensitive to the input error than that of the MODIS LAI product. The performance of the algorithm was also evaluated using fine-resolution LAI maps produced from field LAI measurements and TM data for the Baohe, Maoershan and Hulunbeier regions. The results show that the expanded LAI product differs with field measurements by about 11.5% in the mean LAI values, with agreement to field observations at all three sites to be within 0.8.

Several issues of the MISR LAI product limit the performance of the expanding algorithm such as no valid retrieval in mountainous regions and provisional quality level over needleleaf forest. MISR multi-angle observation is an excellent candidate for the mapping of vegetation structure, such as canopy height, understory reflectance, and clumping index. The expanded LAI can be improved if better LAI products are derived from multi-angular MISR measurements.

Acknowledgment

MISR data were obtained from the NASA Langley Research Center Atmospheric Sciences Data Center and MODIS data from the Land Processes Distributed Active Archive Center. The authors wish to acknowledge the people for their great works in producing these data sets. The authors gratefully acknowledge contributions to the field LAI measurements and fine-resolution LAI maps processing made by Y. Liu, B. Xing, J. Zhu, and G. Zhu of Nanjing University. The authors also would like to thank the anonymous reviewers for their insightful and critical comments, which helped to make this paper be improved largely.

References

[1] J. M. Chen and T. A. Black, "Defining leaf-area index for non-flat leaves," *Plant Cell Environ.*, vol. 15, no. 4, pp. 421–429, May 1992.

[2] J. M. Chen, G. Pavlic, L. Brown, J. Cihlar, S. G. Leblanc, H. P. White, R. J. Hall, D. R. Peddle, D. J. King, J. A. Trofymow, E. Swift, J. Van der Sanden, and P. K. E. Pellikka, "Derivation and validation of Canada-wide coarse-resolution leaf area index maps using high-resolution satellite imagery and ground measurements," *Remote Sens. Environ.*, vol. 80, no. 1, pp. 165–184, Apr. 2002.

[3] R. B. Myneni, S. Hoffman, Y. Knyazikhin, J. L. Privette, J. Glassy, Y. Tian, Y. Wang, X. Song, Y. Zhang, G. R. Smith, A. Lotsch, M. Friedl, J. T. Morisette, P. Votava, R. R. Nemani, and S. W. Running, "Global products of vegetation leaf area and fraction absorbed PAR from year one of MODIS data," *Remote Sens. Environ.*, vol. 83, no. 1/2, pp. 214–231, Nov. 2002.

[4] F. Baret and S. Buis, "Estimating canopy characteristics from remote sensing observations: Review of methods and associated problems," in *Advances in Land Remote Sensing: System, Modeling, Inversion and Application*, S. Liang, Ed. Dordrecht, The Netherlands: Springer-Verlag, 2008, pp. 173–201.

[5] F. Deng, J. M. Chen, S. Plummer, M. Z. Chen, and J. Pisek, "Algorithm for global leaf area index retrieval using satellite imagery," *IEEE Trans. Geosci. Remote Sens.*, vol. 44, no. 8, pp. 2219–2229, Aug. 2006.

[6] F. Baret, O. Hagolle, B. Geiger, P. Bicheron, B. Miras, M. Huc, B. Berthelot, F. Nino, M. Weiss, O. Samain, J. L. Roujean, and M. Leroy, "LAI, fAPAR and fCover CYCLOPES global products derived from VEGETATION—Part 1: Principles of the algorithm," *Remote Sens. Environ.*, vol. 110, no. 3, pp. 275–286, Oct. 2007.

[7] C. Bacour, F. Baret, D. Beal, M. Weiss, and K. Pavageau, "Neural network estimation of LAI, fAPAR, fCover and LAIxC(ab), from top of canopy MERIS reflectance data: Principles and validation," *Remote Sens. Environ.*, vol. 105, no. 4, pp. 313–325, Dec. 2006.

[8] M. J. Chopping, "Terrestrial applications of multiangle remote sensing," in *Advances in Land Remote Sensing: System, Modeling, Inversion and Application*, S. Liang, Ed. Dordrecht, The Netherlands: Springer-Verlag, 2008, pp. 95–144.

[9] D. J. Diner, B. H. Braswell, R. Davies, N. Gobron, J. N. Hu, Y. F. Jin, R. A. Kahn, Y. Knyazikhin, N. Loeb, J. P. Muller, A. W. Nolin, B. Pinty, C. B. Schaaf, G. Seiz, and J. Stroeve, "The value of multiangle measurements for retrieving structurally and radiatively consistent properties of clouds, aerosols, and surfaces," *Remote Sens. Environ.*, vol. 97, no. 4, pp. 495–518, Sep. 2005.

[10] K. Hasegawa, H. Matsuyama, H. Tsuzuki, and T. Sweda, "Improving the estimation of leaf area index by using remotely sensed NDVI with BRDF signatures," *Remote Sens. Environ.*, vol. 114, no. 3, pp. 514–519, Mar. 2010.
[11] G. J. Yang, C. J. Zhao, Q. Liu, W. J. Huang, and J. H. Wang, "Inversion of a radiative transfer model for estimating forest LAI from multisource and multiangular optical remote sensing data," *IEEE Trans. Geosci. Remote Sens.*, vol. 49, no. 3, pp. 988–1000, Mar. 2011.
[12] D. J. Diner, G. P. Asner, R. Davies, Y. Knyazikhin, J. P. Muller, A. W. Nolin, B. Pinty, C. B. Schaaf, and J. Stroeve, "New directions in earth observing: Scientific applications of multiangle remote sensing," *Bull. Amer. Meteorol. Soc.*, vol. 80, no. 11, pp. 2209–2228, Nov. 1999.
[13] Jet Propulsion Lab.California Inst. Technol., D. J. Diner, J. V. Martonchik, C. Borel, S. A. W. Gerstl, H. R. Gordon, Y. Knyazikhin, R. Myneni, B. Pinty, and M. M. Verstraete, MISR Level 2 Surface Retrieval Algorithm Theoretical Basis2008, May.
[14] J. Pisek, J. M. Chen, J. R. Miller, J. R. Freemantle, J. I. Peltoniemi, and A. Simic, "Mapping forest background reflectance in a Boreal region using multiangle compact airborne spectrographic imager data," *IEEE Trans. Geosci. Remote Sens.*, vol. 48, no. 1, pp. 499–510, Jan. 2010.
[15] J. Pisek, J. M. Chen, K. Alikas, and F. Deng, "Impacts of including forest understory brightness and foliage clumping information from multiangular measurements on leaf area index mapping over North America," *J. Geophys. Res.—Biogeosci.*, vol. 115, no. G03 023, p. 13, Sep. 2010.
[16] J. M. Chen and J. Cihlar, "Retrieving leaf area index of boreal conifer forests using landsat TM images," *Remote Sens. Environ.*, vol. 55, no. 2, pp. 153–162, Feb. 1996.
[17] H. Rahman, B. Pinty, and M. M. Verstraete, "Coupled surface-atmosphere reflectance (CSAR) model. 2. Semiempirical surface model usable with NOAA advanced very high-resolution radiometer data," *J. Geophys. Res.—Atmos.*, vol. 98, no. D11, pp. 20 791–20 801, Nov. 1993.
[18] J. N. Hu, Y. Su, B. Tan, D. Huang, W. Z. Yang, M. Schull, M. A. Bull, J. V. Martonchik, D. J. Diner, Y. Knyazikhin, and R. B. Myneni, "Analysis of the MISR LA/FPAR product for spatial and temporal coverage, accuracy and consistency," *Remote Sens. Environ.*, vol. 107, no. 1/2, pp. 334–347, Mar. 2007.
[19] F. Baret and G. Guyot,, "Potentials and limits of vegetation indexes for LAI and APAR assessment," *Remote Sens. Environ.*, vol. 35, no. 2/3, pp. 161–173, Feb./Mar. 1991.
[20] F. Fava, R. Colombo, S. Bocchi, M. Meroni, M. Sitzia, N. Fois, and C. Zucca, "Identification of hyperspectral vegetation indices for Mediterranean pasture characterization," *Int. J. Appl. Earth Observation Geoinf.*, vol. 11, no. 4, pp. 233–243, Aug. 2009.
[21] N. Aparicio, D. Villegas, J. L. Araus, J. Casadesus, and C. Royo, "Relationship between growth traits and spectral vegetation indices in durum wheat," *Crop Sci.*, vol. 42, no. 5, pp. 1547–1555, Sep./Oct. 2002.
[22] M. Spanner, L. Johnson, J. Millera, R. McCreight, J. Freemantle, J. Runyon, and P. Gong, "Remote-sensing of seasonal Leaf-area index across the Oregon transect," *Ecological Appl.*, vol. 4, no. 2, pp. 258–271, May 1994.
[23] J. Heiskanen, "Estimating aboveground tree biomass and leaf area index in a mountain birch forest using ASTER satellite data," *Int. J. Remote Sens.*, vol. 27, no. 5–6, pp. 1135–1158, Mar. 2006.
[24] T. Kraus, M. Schmidt, S. W. Dech, and C. Samimi, "The potential of optical high resolution data for the assessment of leaf area index in East African rainforest ecosystems," *Int. J. Remote Sens.*, vol. 30, no. 19, pp. 5039–5059, 2009.
[25] R. Liu, J. M. Chen, J. Liu, F. Deng, and R. Sun, "Application of a new leaf area index algorithm to China's landmass using MODIS data for carbon cycle research," *J. Environ. Manag.*, vol. 85, no. 3, pp. 649–658, Nov. 2007.
[26] Y. Luo, A. P. Trishchenko, R. Latifovica, and Z. Q. Li, "Surface bidirectional reflectance and albedo properties derived using a land cover-based approach with moderate resolution imaging spectroradiometer observations," *J. Geophys. Res.—Atmos.*, vol. 110, no. D1, p. 17, Jan. 2005.
[27] X. L. Lu, R. G. Liu, J. Y. Liu, and S. L. Liang, "Removal of noise by wavelet method to generate high quality temporal data of terrestrial MODIS products," *Photogramm. Eng. Remote Sens.*, vol. 73, no. 10, pp. 1129–1139, Oct. 2007.
[28] E. Vermote, C. O. Justice, and F. M. Breon, "Towards a generalized approach for correction of the BRDF effect in MODIS directional reflectances," *IEEE Trans. Geosci. Remote Sens.*, vol. 47, no. 3, pp. 898–908, Mar. 2009.
[29] J. M. Chen, "Evaluation of vegetation indices and a modified simple ratio for boreal applications," *Can. J. Remote Sens.*, vol. 22, no. 3, pp. 229–242, Sep. 1996.
[30] M. G. De Kauwe,, M. I. Disney, T. Quaife, P. Lewis, and M. Williams, "An assessment of the MODIS collection 5 leaf area index product for a region of mixed coniferous forest," *Remote Sens. Environ.*, vol. 115, no. 2, pp. 767–780, Feb 2011.
[31] X. F. Chen, J. M. Chen, S. Q. An, and W. M. Ju, "Effects of topography on simulated net primary productivity at landscape scale," *J. Environ. Manag.*, vol. 85, no. 3, pp. 585–596, Nov. 2007.
[32] G. L. Zhu, W. M. Ju, J. M. Chen, W. Y. Fan, Y. L. Zhou, X. F. Li, and M. Z. Li, "Forest canopy leaf are index in Maoershan Mountain: Ground measurement and remote sensing retrieval," (in Chinese), *Chin. J. Appl. Ecology*, vol. 21, no. 8, pp. 2117–2124, Aug. 2010.

Yang Liu (M'10) received the B.S. degree in geographic sciences from the East China Normal University, Shanghai, China, in 2006 and the Ph.D. degree in natural resources from the Institute of Geographic Sciences and Natural Resources Research, Chinese Academy of Sciences, Beijing, China, in 2011.

She is currently a Postdoctoral Research Associate with Beijing Normal University, Beijing. Her research interests cover retrieval of biophysical and atmospheric parameters and global change analysis from remote sensing.

Ronggao Liu (M'10) received the B.S. degree from the Chengdu College of Geology, Chengdu, China, in 1993 and the M.S. degree and Ph.D from the Institute of Geochemistry, Chinese Academy of Science, Guiyang, China, in 1996 and 2000 respectively.

He is currently a Professor with the Institute of Geographical Sciences and Natural Resources Research, Chinese Academy of Sciences. His interests cover algorithms for parameters retrieval and development of processing system for global long-term remote sensing data.

Jing M. Chen received the B.Sc. degree in applied meteorology from the Nanjing Institute of Meteorology, Nanjing, China, in 1982 and the Ph.D. degree in meteorology from Reading University, Reading, U.K., in 1986.

From 1989 to 1993, he was a Postdoctoral Fellow and Research Associate at the University of British Columbia, Vancouver, BC, Canada. From 1993 to 2000, he was a Research Scientist at the Canada Centre for Remote Sensing, Ottawa, ON, Canada. He is currently a Professor and a Canada Research Chair at the Department of Geography, University of Toronto, Toronto, ON. His recent research interests are in the remote sensing of biophysical parameters, plant canopy radiation modeling, terrestrial water and carbon cycle modeling, and atmospheric inverse modeling for global and regional carbon budget estimation. He has published over 120 papers in refereed journals.

Dr. Chen served as an Associate Editor of the IEEE TRANSACTIONS ON GEOSCIENCE AND REMOTE SENSING from 1996 to 2002.

Weimin Ju received the B.Sc. degree from the Nanjing Institute of Meteorology, Nanjing, China, in 1984 and the M.Sc. and Ph.D. degrees from the University of Toronto, Toronto, ON, Canada, in 2002 and 2006, respectively.

He is currently a Professor at the International Institute for Earth System Sciences, Nanjing University, Nanjing, China. His major research interest includes retrieval of vegetation parameters from remote sensing data and simulating terrestrial carbon and water fluxes. He has published over 80 papers in refereed journals, including 34 papers in international journals.